Springer

KSME

Journal of Mechanical Science and Technology 26 (4) (2012) 1027~1041
www.springerlink.com/content/1738-494x
DOI 10.1007/s12206-012-0328-4

Numerical simulation of flow past rectangular cylinders with different aspect ratios using the incompressible lattice Boltzmann method †

S. Ul Islam[1,2], C. Y. Zhou[1,*] A. Shah[2] and P. Xie[1]

[1]*Shenzhen Graduate School, Harbin Institute of Technology, Shenzhen University Town, Shenzhen 518055, China*
[2]*Mathematics Department, COMSATS Institute of Information Technology, Islamabad, Pakistan, 44000*

(Manuscript Received February 16, 2011; Revised May 10, 2011; Accepted October 26, 2011)

Abstract

This paper presents a numerical study of a uniform flow past a rectangular cylinder using the incompressible lattice Boltzmann method (ILBM). Firstly, we use the ILBM to simulate the flow past a square cylinder symmetrically placed in a two-dimensional channel and results are validated against the well-resolved results obtained using finite-difference method and finite-volume method. Secondly, the effects of the aspect ratio defined as R = width/height on the fluid forces, vortex shedding frequency and the flow structures in the wake are investigated. Aspect ratios ranging from 0.15 to 4.00 and four Reynolds numbers Re = 100, 150, 200 and 250 are selected for the investigation. The results show that the effects of aspect ratio on physical quantities such as drag and lift coefficients, Strouhal number and the vortex shedding mechanism are very notable in the range between 0 and 2. In general, the drag coefficient decreases with the aspect ratio and the decreasing rate is more distinct in the range of $0.15 \le R \le 2.0$. There is no local maximum found at around $R = 0.6$ in the drag coefficient as reported for higher Reynolds numbers in the literature. However the root-mean-square value of the lift coefficient shows a maximum value at $R \approx 0.5$ for all Reynolds numbers selected. The variation of Strouhal number with R appears to be different for four selected Reynolds numbers. Especially for Re = 250, a discontinuity in St, as has been observed for higher Reynolds numbers, is observed at around $R = 1.45$ where multiple peaks are found in the result of Fourier spectrum analysis of the lift force and irregular vortex shedding behavior with no fixed shedding frequency is observed from the instantaneous vorticity contours. Such discontinuity is not observed for Re = 100, 150 and 200. The present results using the LBM are compared with some existing experimental data and numerical studies. The comparison shows that the LBM can capture the characteristics of the bluff body flow well and is a useful tool for bluff body flow studies.

Keywords: Aspect ratio effect; Bluff body flow; Incompressible lattice Boltzmann method; Rectangular cylinder

1. Introduction

Bluff structures, for example circular cylinder and rectangular cylinder are the most common configuration in numerous practical applications such as tall buildings, bridges, chimneys, heat exchangers, fences, and so on, and the flow around a bluff body often involves various fluid dynamic phenomena, such as separation, reattachment, and vortex shedding. Therefore the study of bluff body flow is of importance in both engineering and science and has gained attractiveness due to the rapid advance of computer technology and the accuracy of numerical techniques. There have been numerous studies for a circular cylinder and also many investigations for a square cylinder. However, much less work has been conducted for a rectangular cylinder. It is known that the flow around a rectangular cylinder can result in a number of different local instabilities which can lead to global instabilities [1] and the difference in aspect ratio can make drastic changes in the fluid dynamic characteristics around the cylinder [2-4].

Bearman and Trueman [5] conducted an experimental study to examine the flow around rectangular cylinders and their results show that the drag coefficient attains a maximum value at $R \cong 0.62$ for $Re = 0.13 \times 10^5$ and the Strouhal number experiences a discontinuity at R near 2.8. Okajima [6] carried out an experimental study for a rectangular cylinder with the aspect ratio ranging from 1 to 4 where the Reynolds number was in the range from 70 to 2×10^4. He also found that for cylinders with $R = 2.0$ and 3.0 there is a certain range of Reynolds number where an abrupt change of flow pattern occurs with sudden discontinuity in the Strouhal number. For $R = 2.0$ this phenomena happens near $Re = 500$, while for $R = 3.0$ it takes place at about $Re = 1100$. The experimental investigations carried out by Norberg [7] were for the aspect ratios R = 1, 1.6, 2.5 and 3 at various angles of incidence ranging from

*Corresponding author. Tel.: +86 755 2603 3866, Fax.: +86 755 2603 2713
E-mail address: cyzhou@hit.edu.cn
† Recommended by Associate Editor Man-Yeong Ha

0° to 90°. The Reynolds number was in the range of 400 to ~3×10^4. The most notable finding of his work is that the drag coefficient undergoes significant changes in the range of R = 0-1 while the Strouhal number changes very little, whereas the reverse is true in the range of R = 2-3. The drag coefficient reaches a maximum at around R = 0.6. Multiple wake frequencies were observed at some small angles of incidences within a certain range of Re and R between 2 and 3. The experimental work of Nakagawa et al. [8] for a rectangular cylinder in a channel flow was mainly focused on the unsteady turbulence characteristics at Re = 15000. In particular, they observed that in the case of R = 2, the shear layers separate at the leading edges and reattach to the side walls of the cylinder and then separate again at the trailing edges to roll up into regular vortices. However, the simultaneous reattachment to the upper and lower side surfaces occurs intermittently at this aspect ratio, which results in an appearance of narrow and wide width of the wake, and the extent of the recirculation region is largest at this aspect ratio. Recently, Abdollah et al. [9] carried out an experimental study for the same problem but with a smaller blockage ratio. The Reynolds numbers were 8600 and 17400, and the aspect ratios were 0.5, 1.0, 2.0 and 3.0. Their results showed that the Strouhal number remains nearly constant for high Reynolds numbers. They also observed that the vortex formation region is longer in the cases of large aspect ratio than those of lower aspect ratio. Most of these experimental investigations are for fairly high Reynolds numbers, and less information is available for low Reynolds number flows.

Numerical studies of the flow over a rectangular cylinder with different aspect ratios are relatively few. Okajima et al. [10] numerically examined the aspect ratio effects for aspect ratios ranging from 0.4 to 8.0 and Reynolds numbers from 100 to 1.2×10^3 using finite difference methods. They observed some critical changes in flow pattern at R = 2.8 and R = 6.0 at Reynolds numbers of 500 to 1.2×10^3. Kondo and Yamada [11] carried out a third-order upwind finite element study of the flow around rectangular cylinders. Their simulations were carried out for aspect ratios from 0.7 to 4.0 at Re = 10000. Their results show that eddies appearing along the upper and lower surfaces are relatively small when R = 0.7 and 1.0, and, as aspect ratio increases, the formation of vortices around the rectangular cylinders becomes very complex. Sohankar et al. [12, 13] examined the unsteady two-dimensional flow around a rectangular cylinder for different aspect ratios ranging from 0.25-4.00 at various angles of incidences (from 0° to 90°) for Re = 100-200 using the third-order Quick scheme and a second-order Crank-Nicolson scheme. Their results show that there is no local maximum in the drag coefficient at some intermediate critical aspect ratio as observed for higher Reynolds numbers. They also found that the St decreases smoothly with aspect ratio for Re = 100 but increases rather abruptly for Re = 200 at around R = 1.5. But most of their study focused on various numerical parameters such as domain size, grid resolution and time step. Taylor and Vezza [14] studied flow around square and rectangular section cylinders using a discrete vortex method. They observed that a notable effect of aspect ratio on drag coefficient is in the range between 0 and 1 for Re = 20000. Their results showed that a maximum value of drag coefficient is reached at around R = 0.62. The lowest value of R they considered is 0.25. Shimada and Ishihara [15] studied the flow around rectangular cylinders using the k-model for $Re = 2.2\times10^4$ and $0.6 \le R \le 8.0$. Both two- and three-dimensional flows were considered. Their results showed that the drag coefficient experiences a peak near R = 0.6 and then decreases monotonically as the aspect ratio increases. They also observed that St exhibits discontinuities at R = 2.8 and 6.0 for the given Reynolds number. Kevin [16] examined the flow around a square cylinder using the standard lattice Boltzmann method (LBM). The drag coefficient he obtained appears to be higher than those reported by Sohankar et al. [13] while St is in good agreement with those of Sohankar et al. [13]. However, there was limited quantitative information on a rectangular cylinder in his work. Joda et al. [17] carried out an analysis of the forced convection flow around rectangular cylinder with different R using a fractional step finite volume code. Their investigations were carried out for R = 1, 2 and 3 and Re between 100 and 200. Their results showed that the drag coefficient in general decreases with the aspect ratios for Re = 100. For Re = 200 their study on the Strouhal number showed that it first increases and then decreases with the aspect ratio.

As mentioned above there have been some experimental and numerical studies for rectangular cylinders, however, the investigations of the aspect ratio effects on the flow characteristics are still limited, especially for low Reynolds number flows. Quantitative information on aspect ratio effects on vortex structures, the Strouhal number and the force coefficients is far from complete. Regarding the available studies in the literature, the present study provides further computational information and detailed investigation on the aspect ratio effect of a rectangular cylinder at low Reynolds number from 100 to 250 for an aspect ratio ranging from 0.15 to 4.00. The effects of the aspewct ratio on the force coefficients, the Strouhal number and the flow structures in the near wake are studied in detail. The LBM with the incompressible Bhatnagar-Gross-Krook (LBGK) [18] model is used for the fluid flow simulation and the results are compared with related data published in the literature.

The rest of the paper is organized as follows: A brief description of the problem is given in section 2 and a detailed description of the incompressible lattice Boltzmann method (ILBM) together with the initial and boundary conditions and the validation test for the numerical code are presented in section 3. The results on the effects of the aspect ratio on the force coefficients, vortex shedding frequency and the flow structures are discussed in section 4. The effects of the Reynolds number are also given in this section. Finally conclusions are drawn in Section 5.

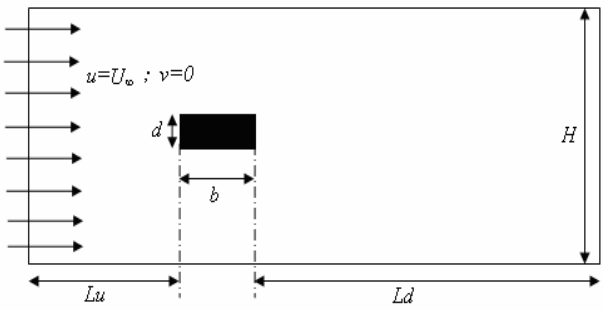

Fig. 1. Schematic configuration of a rectangular cylinder in a uniform flow.

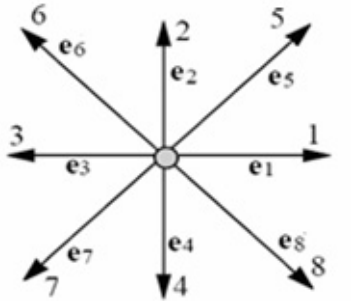

Fig. 2. Two-dimensional nine-velocity lattice (D2Q9) model.

2. Problem description

The schematic configuration of a rectangular cylinder in a uniform flow is shown in Fig. 1, where d and b are the side width and length of the cylinder, and U_∞ is the velocity of the uniform flow. H is the height of the computational domain. A computational domain with $L_u = 12d$ upstream, $L_d = 30d$ downstream and a distance of $H = 12d$ on both sides of the cylinder is selected for the present computations, and has been proven to provide a good compromise between accuracy of the solution and computational cost for a uniform flow past a cylinder as will be shown later.

3. Numerical method

3.1 Incompressible lattice Bhatnagar-Gross-Krook (ILBGK) model

Instead of solving the usual continuum equations for the conserved fluid fields, the lattice Boltzmann method (LBM) models the fluid flow by tracking the evolution of fluid particles where the physical space is discretized into a number of square regular lattices and at each time step, the particles move and collide following certain rules. In the present study, a two-dimensional nine-velocity (D2Q9) model and the Bhatnagar-Gross-Krook (BGK) collision model used in the standard Boltzmann equation are adopted [19].

The evolution equation of the density distribution function of the fluid particles can be described by:

$$g_i(\boldsymbol{x} + c\boldsymbol{e}_i\Delta t, t + \Delta t) - g_i(\boldsymbol{x}, t) = \Omega_i(g) \tag{1}$$

where $g_i(\boldsymbol{x},t)$ is the density distribution function of the particle at position $\boldsymbol{x}$ and time t with velocity $c\boldsymbol{e}_i$, Δx and Δt are the lattice grid spacing and the time step, $c = \Delta x/\Delta t$ is the particle speed, $\boldsymbol{e}_i$ is the direction of the velocity, and Ω_i is the collision operator which must maintain the total mass and momentum of the particle system. The fluid density ρ is then obtained from the density distribution function by:

$$\rho = \sum_i g_i \,. \tag{2}$$

The density distribution function $g_i(\boldsymbol{x},t)$ is modified at each time step according to the evolution of the particles.

In the two-dimensional nine-velocity (D2Q9) model, each lattice node has eight nearest neighbors connected by eight links and the particles move only along the axes or the diagonal directions of the lattice (see Fig. 2). The directions of the discrete velocities are given by:

$$\boldsymbol{e}_i = \begin{cases} (0,0); & i = 0 \\ (\cos|(i-1)\pi/2|, \\ \sin|(i-1)\pi/2|); & i = 1,2,3,4 \\ \sqrt{2}(\cos|(i-5)\pi/2+\pi/4|, \\ \sin|(i-5)\pi/2+\pi/4|); & i = 5,6,7,8 \end{cases} . \tag{3}$$

Bhatnagar, Gross and Krook (BGK) (1954) described a collision operator to consider the collision effects between particles where the collision process was described as a relaxation to the local equilibrium state in the following way:

$$\Omega_i = -\frac{1}{\tau}[g_i(\boldsymbol{x},t) - g_i^{(0)}(\boldsymbol{x},t)] \tag{4}$$

where τ is the non-dimensional relaxation and $g_i^{(0)}(\boldsymbol{x},t)$ is an equilibrium distribution function. The equilibrium distribution chosen by Guo et al. [19] is defined by:

$$g_i^{(0)}(\boldsymbol{x},t) = \alpha_i p + \omega_i \left[3\frac{(\boldsymbol{e}_i \cdot \boldsymbol{u})}{c} + 4.5\frac{(\boldsymbol{e}_i \cdot \boldsymbol{u})^2}{c^2} - 1.5\frac{|\boldsymbol{u}|^2}{c^2} \right] \tag{5}$$

where:

$$\alpha_i = \begin{cases} -4\dfrac{\sigma}{c^2} & i = 0 \\ \dfrac{\lambda}{c^2} & i = 1,2,3,4 \\ \dfrac{\gamma}{c^2} & i = 5,6,7,8 \end{cases} \quad \text{and}$$

$$\omega_i = \begin{cases} 4/9 & i = 0 \\ 1/9 & i = 1,2,3,4 \\ 1/36 & i = 5,6,7,8 \end{cases} \quad (6)$$

and σ, λ, γ are parameters satisfying λ + γ = σ and λ + 2γ = 1/2.

The evolution equation of the density distribution function is then described by the following single-relaxation-time BGK equation:

$$g_i(\boldsymbol{x} + c\boldsymbol{e}_i\Delta t, t + \Delta t) = g_i(\boldsymbol{x},t) - \frac{1}{\tau}[g_i(\boldsymbol{x},t) - g_i^{(0)}(\boldsymbol{x},t)] \quad (i = 0,1,2,\ldots,8). \quad (7)$$

The incompressible Navier–Stokes equations can be recovered from this incompressible LBGK model [19, 20].

The kinematic viscosity ν can be obtained in the following way:

$$\nu = c_S^2\left(\tau - \frac{1}{2}\right)\frac{(\Delta x)^2}{\Delta t} \quad (8)$$

where $cs = c/\sqrt{3}$ is the speed of sound. A careful selection of τ is very important in lattice Boltzmann (LB) modeling since the numerical stability and computational cost depend on the value of τ. The flow velocity and pressure can be obtained by

$$\boldsymbol{u} = \sum_{i=1}^{8} c\boldsymbol{e}_i g_i \quad (9)$$

$$p = \frac{c^2}{4\sigma}\left[\sum_{i=1}^{8} g_i - \frac{2|\boldsymbol{u}|^2}{3c^2}\right]. \quad (10)$$

More details can be found in Ref. [19].

3.2 Boundary conditions

Inlet boundary: Uniform flow with velocity U_∞ is incorporated using the equilibrium particle distribution function (PDF) at the inlet boundary where

$$u = U_\infty \quad \text{and} \quad v = 0. \quad (11)$$

Outlet boundary: The computational domain behind the cylinder is selected to be large enough so that the flow at the outflow boundary can be considered to be fully developed. Therefore a zeroth order approximation for PDF is adopted at the outlet boundary.

Surface of the cylinder: No-slip wall boundary condition is applied to the surface, i.e.

$$u = 0 \quad \text{and} \quad v = 0 \quad (12)$$

and this is realized using a bounce-back treatment in which all particles hitting the solid wall and reflected back to its previous position.

Top and bottom boundaries: Uniform flow boundary condition is applied at both top and bottom boundaries of the computational domain.

$$u = U_\infty \quad \text{and} \quad v = 0 \quad (13)$$

The total fluid force F on the square cylinder is calculated using the momentum exchange method [21]. The force is given by:

$$F = \sum_{all\ x_b}\sum_{\alpha=1}^{N} e_\beta[n_\alpha(x_b, t) + n_\alpha(x_b + e_\beta\Delta t, t)]\frac{\Delta x}{\Delta t} \quad (14)$$

where N is the number of non-zero lattice velocity vectors, the subscript α is the opposite lattice direction of β, i.e. $\alpha = \beta = 1,2,\ldots,8$. To obtain the fluid-solid momentum exchange per unit time, Eq. (14) is treated at the midpoint for the fluid lattice node $x_f = (x_b + ce_\beta\Delta t,\ t)$ and the solid lattice node $x_b = (x_f + ce_\alpha\Delta t,\ t)$, where x_b denotes the solid nodes and x_f represents the fluid nodes. The momentum exchange between a solid node at x_b and all possible neighboring fluid nodes around that solid node can be obtained by the inner summation, while the force contribution for all boundary nodes at x_b is given by the outer summation.

3.3 Definition of important parameters

The Reynolds number Re is defined by:

$$Re = U_\infty d/\nu. \quad (15)$$

Other important parameters are the Strouhal number *St*, the drag coefficient *Cd*, the lift coefficient *Cl*, and aspect ratio *R*. They are defined by the following formulas:

$$St = f_S d/U_\infty \quad (16)$$

$$Cd = \frac{F_d}{\frac{1}{2}\rho U_\infty d} \quad (17)$$

$$Cl = \frac{F_l}{\frac{1}{2}\rho U_\infty^2 d} \quad (18)$$

$$R = \frac{b}{d} \quad (19)$$

where f_s is the vortex shedding frequency from the cylinder, F_d and F_l are the force components in the in-line and transverse directions, respectively.

Computations are normally terminated when the following

convergence criteria is satisfied

$$\frac{\sqrt{\sum_{l,m}[u_{l,m}^{(k+1)}-u_{l,m}^{(k)}]^2}}{\sqrt{\sum_{l,m}[u_{l,m}^{(k+1)}]^2}} \le 1\times10^{-6} . \quad (20)$$

All the computations are carried out on a Dawning Parallel Computer TC4000.

3.4 Computer code validation

In order to validate the computer code, simulations for flow past a square cylinder are carried out first for Re = 100, 150, 200 and 250. The results of C_{dmean}, the mean value of drag coefficient, and the Strouhal number St are presented together with the experimental data of Shimuzu and Tanida [22], Okajima [6], Okajima [23] and Norberg [7] in Figs. 3 and 4, respectively. Some numerical results of Davis and Moore [24], Franke et al. [25], Sohankar et al. [26], Robichuax et al. [27] and Saha et al. [28] are also plotted in the figure for comparison. It is seen that the present calculation for the mean drag coefficient at Re = 250 is very close to the experimental data of Shimizu and Tanida [22]. It is also observed that the present calculation for Cd_{mean} at Re = 200 is very close to the numerical result of Sohankar et al. [26]. The present results at this Reynolds number show a much better prediction than other numerical data as seen in the figure. However the present study underpredicts the drag coefficient for Re = 100. Although most of the numerical data illustrate an underprediction at this Reynolds number, the present work shows more. The general trend from all of the numerical studies is similar, and the present result agrees well with that from Sohankar et al. [26] who used the Quick scheme and Van Leer scheme, but is lower than numerical solutions by others. The Strouhal numbers obtained in the present work show a good agreement with some of the data from Norberg [7] and Okajima [6]. The present Strouhal number and those obtained by Franke et al. [25] shows a similar trend for the variation of the Strouhal number with Re.

4. Results and Discussion

Four Reynolds numbers 100, 150, 200 and 250 are considered. In order to investigate the effects of the aspect ratio, twenty-six values of R between 0.15 and 4 are selected for each of the Reynolds numbers. The values are listed in Table 1. The drag and lift coefficients, the vortex shedding frequency and the flow structure are analyzed. The effects of Reynolds number are also examined.

4.1 Drag and lift force coefficients

For the sake of brevity, only two groups of force time histories are presented. The first one is illustrated in Fig. 5 where R varies from 0.15 to 4 and Re is kept at 100. The second one is plotted in Fig. 6 where Re varies from 100 to 250 and R is kept at 0.5. The solid line represents the drag coefficient and the dotted line indicates the lift coefficient. The time history of the drag and lift coefficients exhibit regular periodic behaviors which indicates the periodic alternate vortex shedding phenomenon. It is seen that the periodic vortex shedding behavior is well captured by the LBM method. The frequency of the drag coefficient is twice that of the lift coefficient. The fluctuations of Cd and Cl become smaller with the increase of R (see Fig. 5(a)-(d)) and larger as Re is increased (see Fig. 6(a)-(d)).

The mean value of the drag coefficient, C_{dmean}, is presented in Fig. 7 as a function of R. A notable effect of aspect ratio on C_{dmean} in the range between 0 and 1 is observed in the figure,

Table 1. Aspect ratios selected.

0.15	0.25	0.40	0.45	0.50	0.55	0.60
0.75	0.90	1.00	1.25	1.40	1.45	1.50
1.60	1.70	1.75	2.00	2.25	2.50	2.75
3.00	3.25	3.50	3.75	4.00		

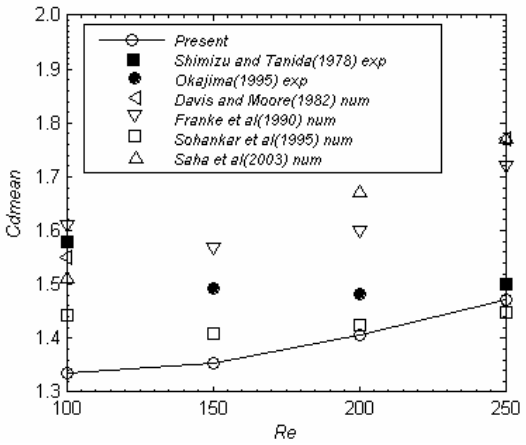

Fig. 3. Comparison of the drag coefficient between present results and some data published in literature for flow past a square cylinder.

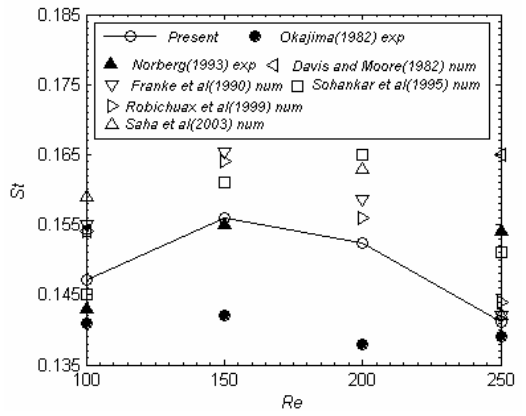

Fig. 4. Comparison of the Strouhal number between present results and some data published in literature for flow past an square cylinder.

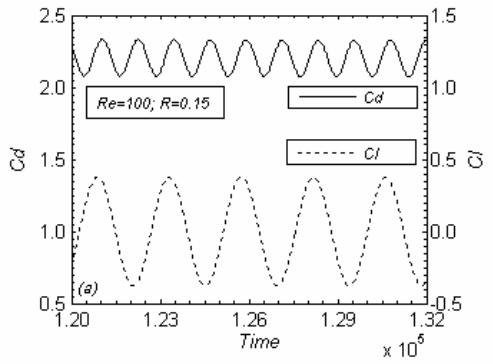

(a) $R = 0.15$

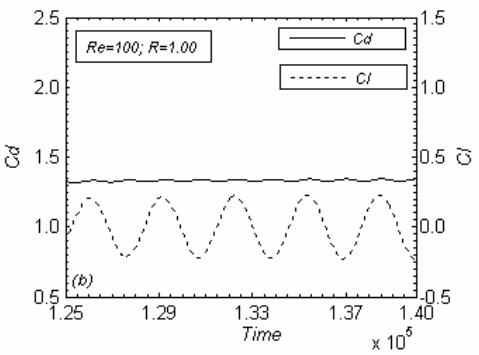

(b) $R = 1.0$

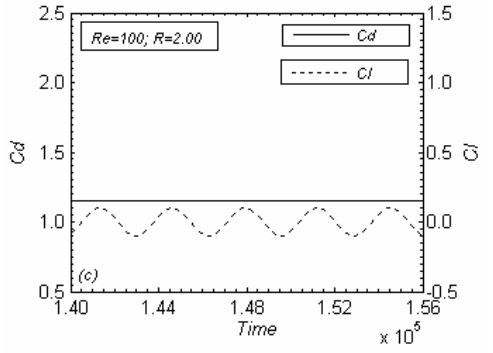

(c) $R = 2.0$

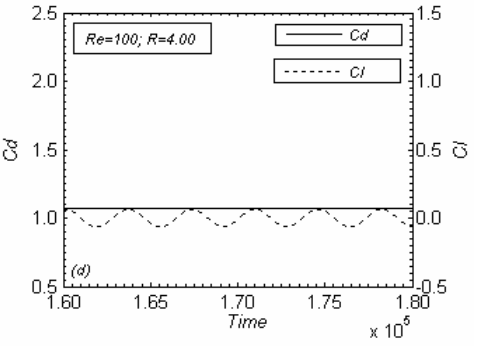

(d) $R = 4.0$

Fig. 5. Variation of lift and drag coefficient for different aspect ratio at $Re = 100$.

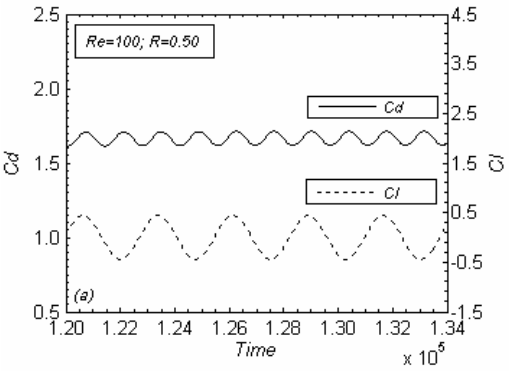

(a) $Re = 100$

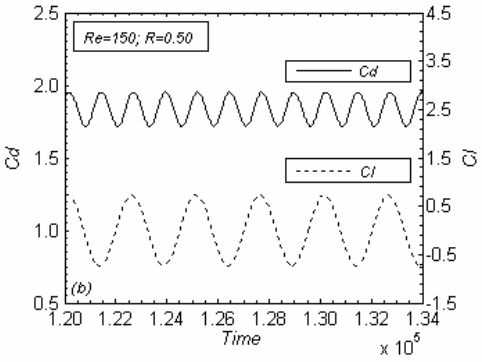

(b) $Re = 150$

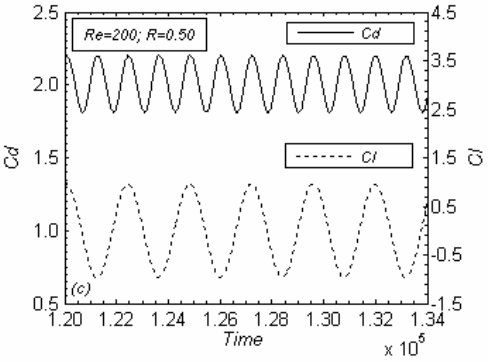

(c) $Re = 200$

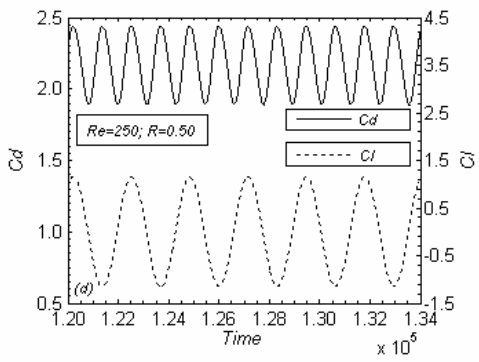

(d) $Re = 250$

Fig. 6. Variation of lift and drag coefficient for different Re where $R = 0.5$.

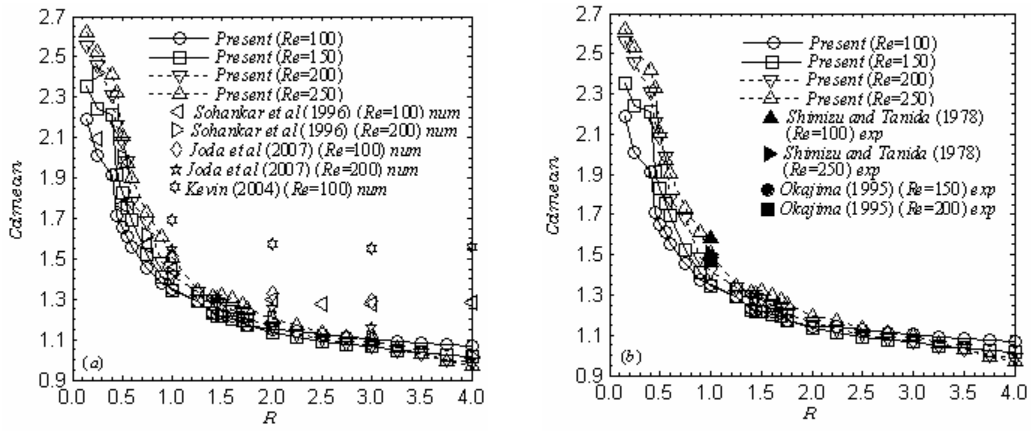

(a) Comparison with other numerical results (b) Comparison with experimental results

Fig. 7. Mean drag coefficient as a function of R for different Reynolds numbers.

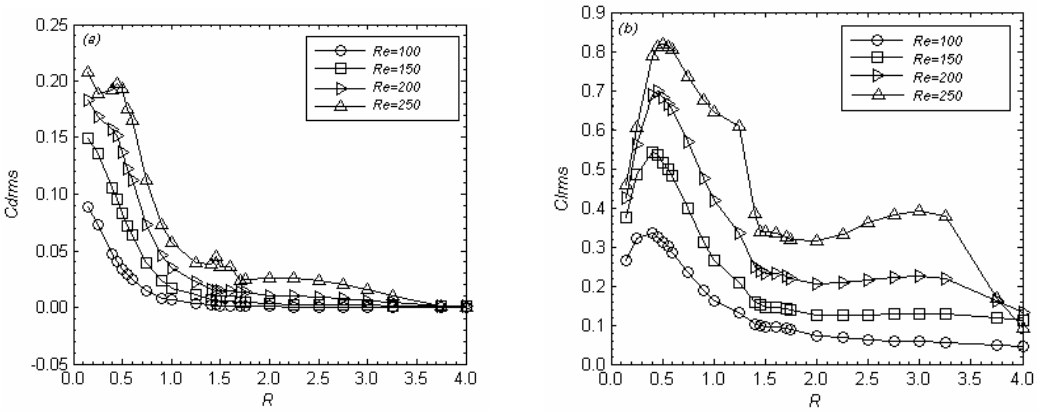

(a) Root-mean-square value of drag coefficient (b) Root-mean-square value of lift coefficient

Fig. 8. Variations of the root-mean-square values of drag and lift coefficients with the aspect ratio R.

which is consistent with the observations reported in the literature [7, 12, 14]. It is seen that for all selected Reynolds numbers, C_{dmean} drops sharply as R increases when $R < 1$, and when $R > 1$ it decreases slowly. There is a slight increase at $R = 3.5$ for $Re = 100$ and 200. When R varies from 0.15 to 4.0, the drag coefficient is reduced by up to 54.3% for $Re = 100$, 60.6% for $Re = 150$, 62.9% for $Re = 200$ and 64.8% for $Re = 250$. In order to capture very detailed information on the behaviors of the force coefficients and also the Strouhal number as a function of the aspect ratio, a large number of computations for a series of carefully selected aspect ratios were carried out. The local maximum value in drag coefficient at some intermediate critical aspect ratio as observed for higher Reynolds numbers [5, 7, 14, 15] is not observed for the present low Reynolds numbers. However a maximum value in the lift coefficient appears at these low Reynolds numbers as will be seen in the following. For comparison, the experimental results of Shimizu and Tanida [22] and Okajima [23] and the computational results of Sohankar et al. [12], Kevin [16] and Joda et al. [17] are also presented in the figure. The results of Sohankar et al. [12] lie closely on the present results. The results of Kavin [16] who also used the LBM appear to be generally higher than those of all others. The present results show that the C_{dmean} is slightly lower than those reported by Shimizu and Tanida [22] and Okajima [23] though the comparison shows a generally good agreement between the experimental data and the computational results.

The root-mean-square values of drag and lift coefficients, C_{drms} and C_{lrms}, are illustrated in Fig. 8(a) and (b), respectively. The variation of C_{drms} with R shows a similar trend to its mean value but with a more distinct decreasing rate in the range of $R < 1.5$ for all selected Re. It remains nearly a constant for $R > 1.5$. Therefore the results indicate that large aspect ratio effects on the drag coefficient appear only when R is smaller than 1. However the rms value of the lift coefficient behaves differently. It increases sharply as R increases from $R = 0.15$ and reaches a maximum values at around $R \approx 0.5$ for all selected Reynolds numbers. It then decreases quickly as R increases to 1.5. When R is greater than 1.5, C_{lrms} remains nearly a constant for Reynolds number 100, 150, and 200. But for $Re = 250$, C_{lrms} starts to increase with R after the decrease from a peak value at $R = 0.5$ and reaches another peak at $R = 3.0$.

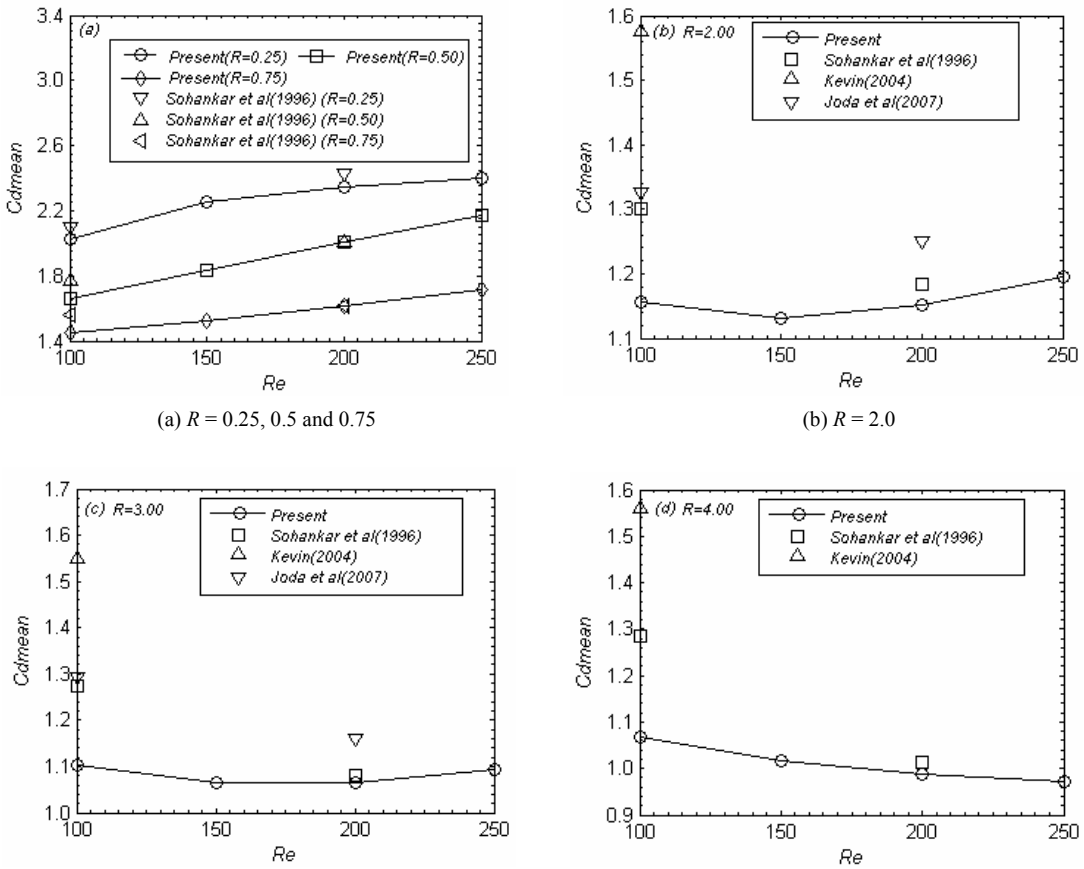

(a) R = 0.25, 0.5 and 0.75 (b) R = 2.0

(c) R = 3.0 (d) R = 4.0

Fig. 9. Variation of drag coefficients as a function of *Re* for fixed aspect ratios.

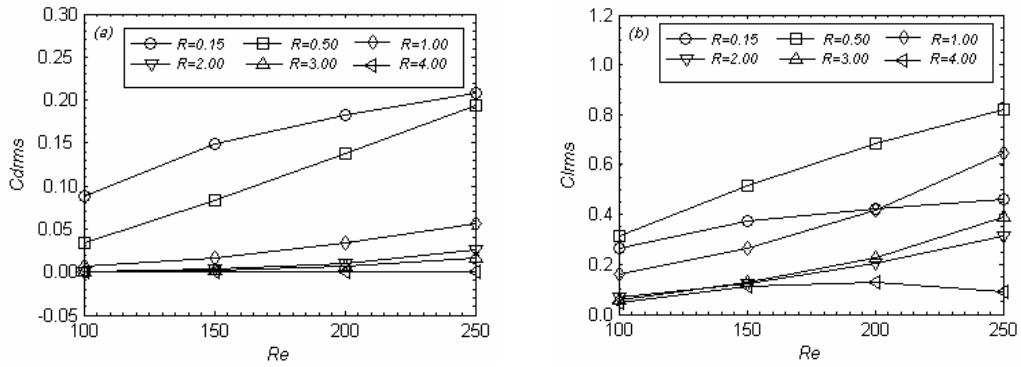

(a) The rms drag coefficient (b) The rms lift coefficient

Fig. 10. Variations of the root-mean-square (rms) values of lift and drag coefficients as a function of *Re* for fixed aspect ratios.

After that it drops quickly down to a value close to the values for all other selected *Re*. As the Reynolds number increases, the behavior of C_{lrms} becomes more complicated.

To illustrate the influence of the Reynolds number, the results of C_{dmean}, C_{drms} and C_{lrms} are illustrated for fixed aspect ratios. Fig. 9 shows the variations of C_{dmean} for R = 0.25, 0.5, 0.75, 2, 3 and 4 with the Reynolds number. Some open literature data are also put in the figure for comparison. The mean value of drag coefficient increases with *Re* for the aspect ratios $R \le 1$, but in the range of $1<R<4$ the drag coefficient changes only slightly with *Re* for a fixed aspect ratio and the variation is within 7% (see Fig. 9(b), (c) and (d)).

Fig. 10 summarizes the variations of the root-mean-square values of the drag and lift coefficients with Reynolds number in the range of *Re* from 100 to 250 for fixed aspect ratios. It is seen that except for the case of R = 4 and Re = 250, the root-mean-square values of the drag and lift coefficients generally increase with *Re* for the ranges of R and *Re* considered. At

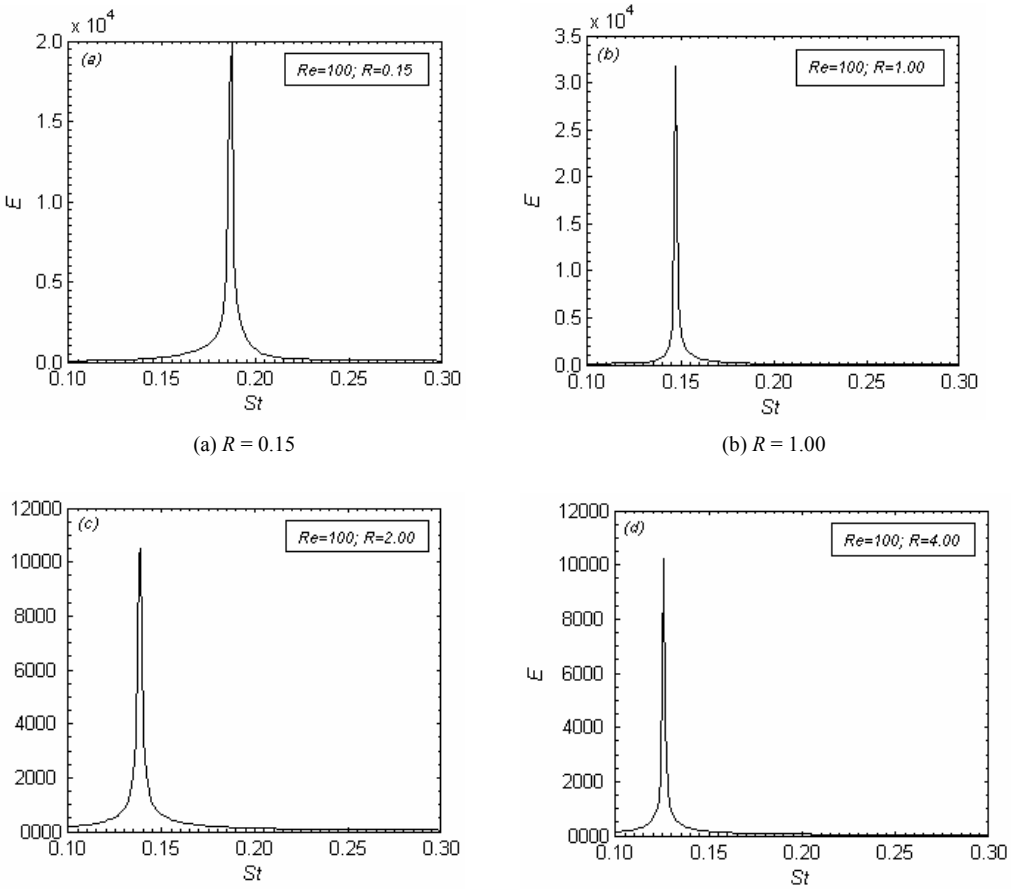

(a) R = 0.15 (b) R = 1.00

(c) R = 2.00 (d) R = 4.00

Fig. 11. Fourier spectrum analysis of lift coefficient for different aspect ratio at Re=100.

R = 4 and Re = 250, C_{lrms} shows a slight decrease.

4.2 Vortex shedding frequency

Fourier spectrum analysis of the lift coefficients are carried out for all R and Re to analyze the vortex shedding frequency. The results for four selected cases with a fixed value of Re = 100 are illustrated in Fig. 11. All of the four graphs show a single dominant peak which relates to the vortex shedding frequency. The vortex shedding becomes slower as the aspect ratio increases at this Reynolds number.

More detailed variations of St with aspect ratio R for the selected four Reynolds numbers are summarized in Fig. 12. Some experimental and numerical data published in the literature are also given in the figure for comparison. For Re = 100, Fig. 12(a) shows that St decreases quickly with R first when R < 1 and then steadily with a slower decreasing rate for R > 1, while for Re = 150, 200 and 250 the Strouhal number increases initially and reaches a peak at around R = 0.25, 0.45 and 0.50 for Re = 150, 200 and 250, respectively. It then drops sharply and meets a minimum at around R = 1.0 and 1.25 for Re = 150 and 200, respectively. However, for Re = 250 the Strouhal number experiences a drastic change at the aspect ratios of 1.40, 1.45 and 1.50. With these aspect ratios the vortices shed irregularly with no fixed shedding frequencies, which may be seen from the flow patterns shown in the next subsection and the results of Fourier spectrum analysis of the lift forces, which show multiple peaks with no obvious dominant one (see Fig. 13). Therefore there appears to be a discontinuity in the Strouhal number as shown in Fig. 12(d).

It is known that the Strouhal number experiences a discontinuity at some aspect ratios for a certain range of Reynolds number where an abrupt change of flow pattern occurs [5-7, 15]. It has been reported that this discontinuity happens at R = 2 for Re near 500 and at R = 3.0 for Re near 1100 by Okajima [6]. For a lower Reynolds number Re = 250, this discontinuity is expected to occur at an aspect ratio lower than 2. The drastic change at around R = 1.45 shown in Fig. 12(d) illustrates the occurrence of such a discontinuity in the Strouhal number for Re = 250 as expected. For Re = 200 or even lower, this discontinuity is not observed in the present study.

The comparison of the present results with those published data indicates that some of the present results are in reasonable agreement with the experimental results of Okajima [6], Norberg [7] and Nakamura et al. [4], for example, for Re = 100. But for other Reynolds numbers, some of the results are scat-

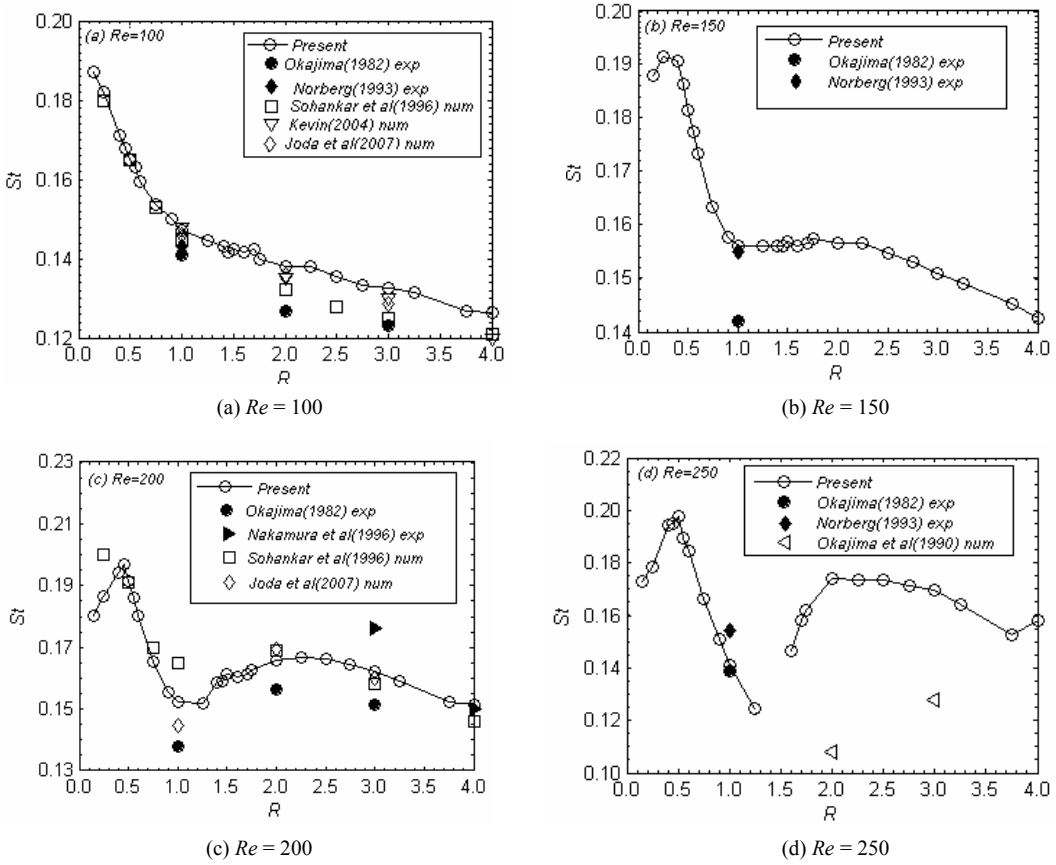

(a) Re = 100 (b) Re = 150

(c) Re = 200 (d) Re = 250

Fig. 12. Strouhal number as a function of the aspect ratio for different Reynolds numbers.

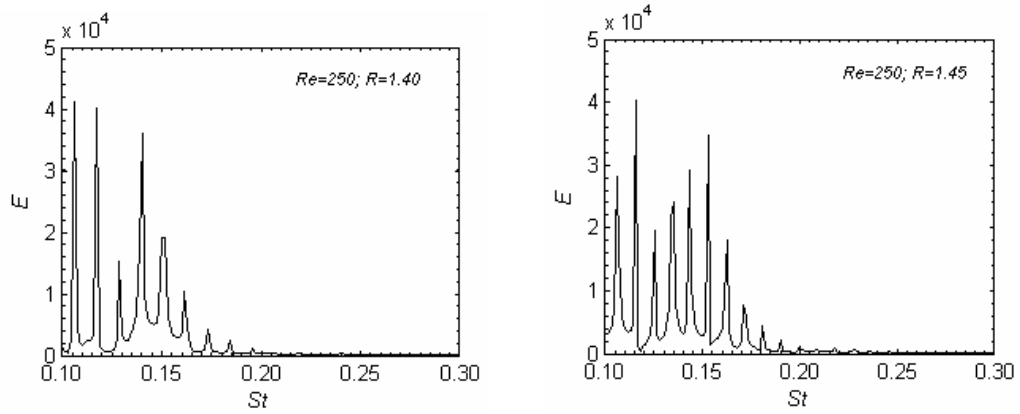

(a) R = 1.4 (b) R = 1.45

Fig. 13. Fourier spectrum analysis of lift coefficient at different aspect ratio with Re = 250.

tered. The agreement between the present results and the data of Norberg [7] is generally better than the agreement with the data of Okajima [6] and Nakamura et al. [4].

Fig. 14 shows the variation of St with Re. Some published data from other experimental and numerical investigations [4, 6, 7, 13, 16, 17] are also included for comparison. It can be seen that some of the present results are close to the experimental data reported by Okajima [6] and Norberg [7], for example, for R = 1 at Re = 100 and 150 to the data of Norberg [7] and at Re = 250 to that of Okajima [6], and for R = 4 at Re = 200 to the data of Nakamura et al. [4]. The present results show that when $R > 1$, the Strouhal number generally increases with Re for the Reynolds number range tested.

4.3 Flow structures in the wake

Instantaneous vorticity contours are used to visualize the flow structures and they are presented in Fig. 15-18 for

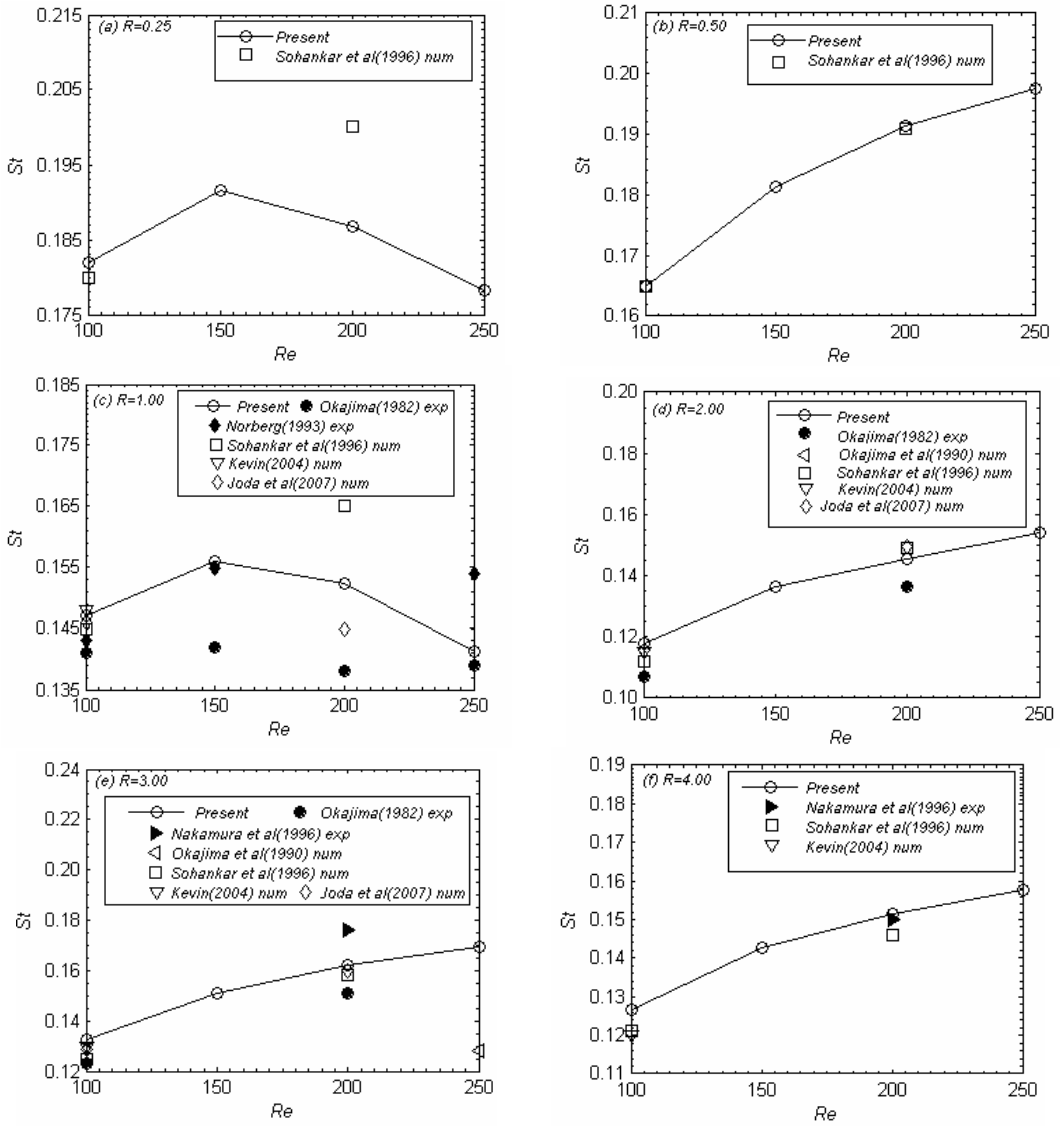

Fig. 14. Variation of *St* as a function of Reynolds numbers for flow past a rectangular cylinder with different aspect ratio.

Re = 100, 150, 200 and 250, respectively. Negative vorticity (clockwise vortex) is shown by dashed lines and the positive vorticity (anticlockwise vortex) by solid lines. In general, all the figures show that the shear layer on one side is rolling up to form a vortex while another vortex with opposite sign on the other side is about to shed. The vortices shed from the upper and lower sides of the cylinder alternatively and then are swept downstream. However the vortex patterns around the cylinder change greatly as the aspect ratio varies from 0.15 to 4 for each value of *Re* examined.

Fig. 15 shows the comparison of the vortex pattern for different aspect ratios at *Re* = 100. The results indicate that at a low aspect ratio of *R* = 0.15 the flow structure behind the cylinder has a form of two parallel lines with negative and positive vortices respectively (see Fig. 15(a)). At an aspect ratio of *R* = 0.50, the vortices shed alternatively from the upper and lower sides of the cylinder to form a typical Kaman vortex street with a relatively short formation length (see Fig. 15(b)). Fig. 15(c) shows that the negative vortex is being shed and the positive one on the other side is reforming. The vortex on one side draws the shear layer of opposite sign from the other side across the wake centerline to detach the vortex from the near wake and form the vortex street. Similar patterns are noted in Fig. 15(d)-(f).

However, as the aspect ratio increases the vortex formation length, the width of the near wake, and the spacing between vortices in both the transverse and stream directions change greatly. It is observed that the formation length becomes longer as the aspect ratio increases, for example, the one in Fig. 15(f) for *R* = 4.00 is longer than that in Fig. 15(b) for a lower value of *R* = 0.50. This is also observed for higher Reynolds numbers, e.g. Abdollah [9] for *Re* = 8600 and 17400 for different aspect ratios. It is seen from Fig. 15 that the width of the near wake becomes narrower as the aspect ratio increases

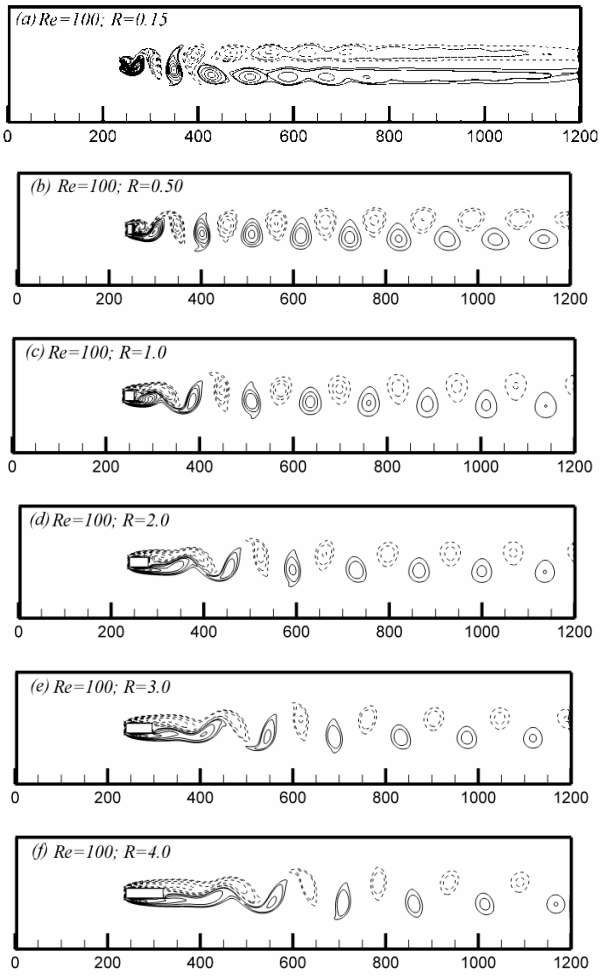

Fig. 15 Vorticity contours around rectangular cylinders with different aspect ratios at Re = 100.

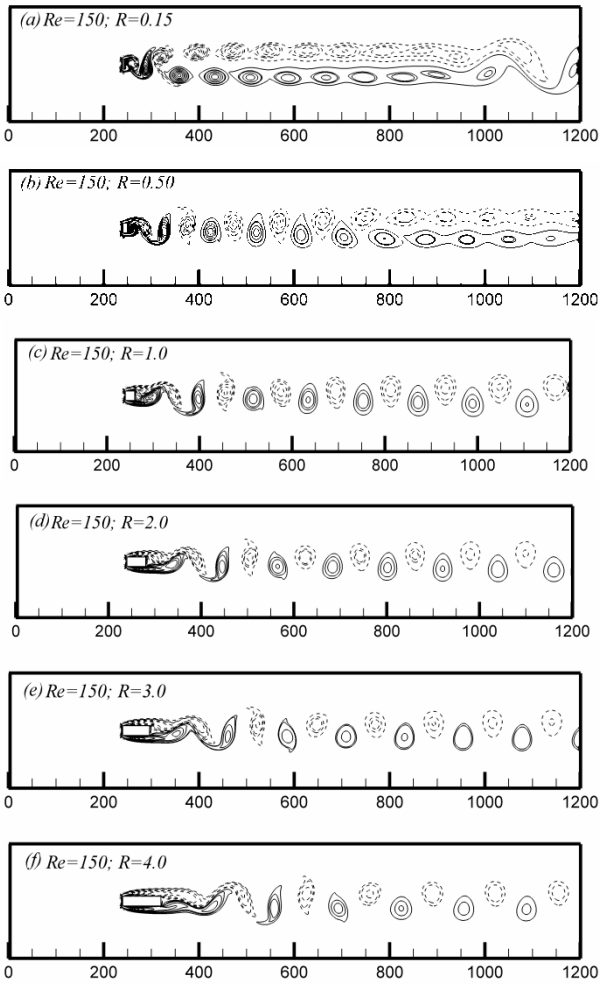

Fig. 16. Vorticity contours around rectangular cylinders with different aspect ratios at Re = 150.

which results in the decrease in the drag coefficient shown in Fig. 7. The spacing between vortices in the stream direction increases, which indicates that the vortices shed more slowly as the aspect ratio increases for a fixed Reynolds number. This is accompanied by a decrease in the vortex shedding frequency as shown in Fig. 12(a).

The formation of vorticity contours behind the rectangular cylinder for different aspect ratios at Re = 150 is shown in Fig. 16. Similar to the cases for Re = 100, the result for R = 0.15 shows a quite steady form of two parallel lines with negative and positive vortices (see Fig. 16(a)). A positive vortex is in the process of development on lower side of the cylinder, while a negative vortex is about to detach from the cylinder (Fig. 16(b)). Fig. 16(c)-(f) show that the negative vortex has cut off the connection between the lower shear layer and the positive vortex, and the near wake region is larger in the cases with large aspect ratios. Similar changes in vortex spacing and wake width to those found for Re = 100 are observed here for Re = 150. Fig. 17 shows the vortex patterns for different aspect ratios at Re = 200. The flow patterns for R = 0.15 are much more complicated as compared to those for Re = 100 and 150, as shown in Fig. 17(a). It is seen that the two parallel lines with negative and positive vortices do not persist long before becoming unstable. The two parallel lines of vortices, while they travel downstream with the stream, start pairing and rolling up after a distance of three pairs of shedding vortices. However a quite steady form of two parallel lines with negative and positive vortices is seen in the wake of the cylinder for R = 0.5 (see Fig. 17(b)). It is seen that as R is increased further, the vortex shed from one side crosses the wake centerline eventually and cuts the supply of vorticity to the vortex shed from the other side, and draws the shear layer of opposite sign from the other side to form the typical Kaman vortex street (Fig. 17(c)-(f)). Fig. 17(d) shows that the negative vortex is being shed and the positive one on the other side is reforming. From the vortex patterns shown in Fig. 17(e) for the aspect ratio 4.00, it can be seen that the wake region is longer as compared to those of other aspect ratios.

Fig. 18 shows the vorticity contours for different aspect ratios at Re = 250. The flow field for R = 0.15 and 0.5 at

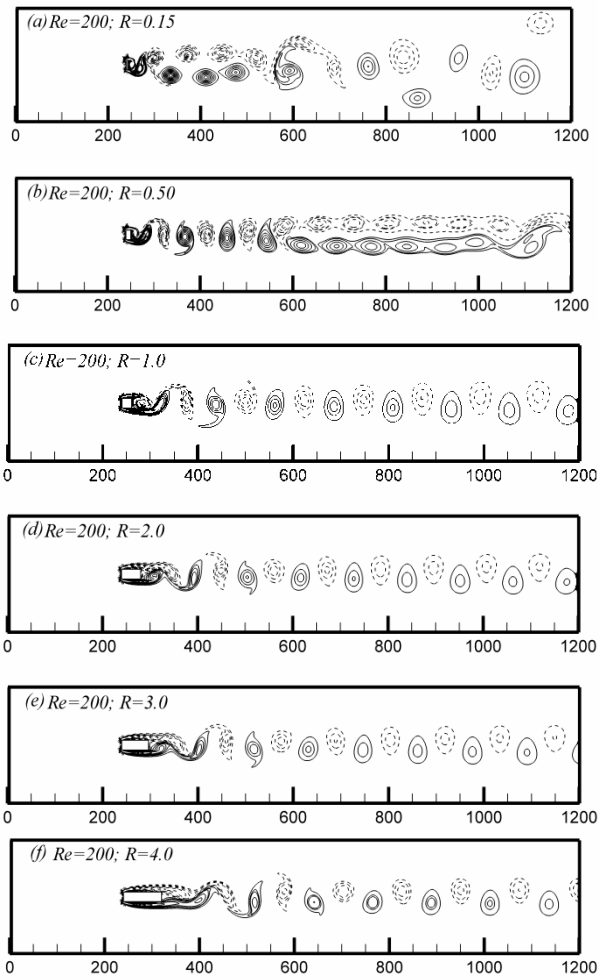

Fig. 17. Vorticity contours around rectangular cylinders with different aspect ratios at Re = 200.

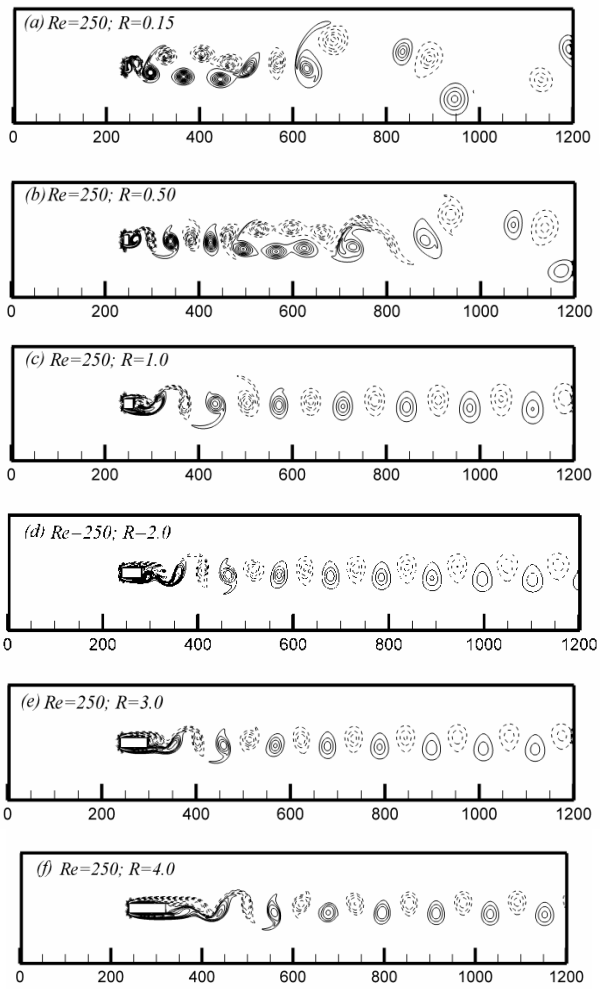

Fig. 18. Vorticity contours around rectangular cylinders with different aspect ratios at Re = 250.

Re = 250 is more complicated, as shown in Fig. 18(a) and (b). The vortex shedding process is affected greatly by the horizontal length of the cylinder. When the horizontal length is short, the separation flows from the trailing edges of the cylinder are sucked into the back region of the cylinder immediately at this Reynolds number. As a result the vortices generated on one side immediately interact with those of opposite sign which are in the process of being formed on the other side of the cylinder, and cut the supply of vorticity to the vortex shed from the other side. It is seen that the vortex shed at a position very close to the cylinder (see Fig. 18(a) and (b)), and shedding frequency is relatively high (see Fig. 12(d)). The positive and negative vortices move downstream with different velocities and interact in the wake and partially annihilate each other's vorticity (see Fig. 12(d)). Figs. 18(c)-(f) show typical Kaman vortex street patterns. The spaces between the vortices in the in-line direction for R = 1 and 4 are obviously larger than those for R = 2 and 3 which indicate that the vortex shedding frequency for these two cases are slower (see Fig. 12(d)), but in each of these cases the spaces between consecutive vortices remain almost a constant. The near-wake region is longer in the cases of larger aspect ratios compared to that of lower aspect ratios (see Fig. 18(d)-(f)).

To further analyze the flow structures in the range of discontinuity where the results of FFT spectrum analysis of lift coefficient show multiple peaks, vorticity contours at two different times for R = 1.40, 1.45 and 1.50 are illustrated in Fig. 19. It is obviously seen that in each of these three cases there is no a fixed vortex shedding frequency and the space between consecutive vortices in the streamwise direction changes irregularly. This is why multiple peaks in the FFT spectrum analysis are found (see Fig. 12(d)).

5. Conclusion

The flow characteristics around a rectangular cylinder with different aspect ratios in a uniform flow are studied using the lattice Boltzmann method (LBM) with the incompressible Bhatnagar-Gross-Krook (LBGK) model. Aspect ratios ranging from 0.15 to 4.00 are selected and four Reynolds numbers

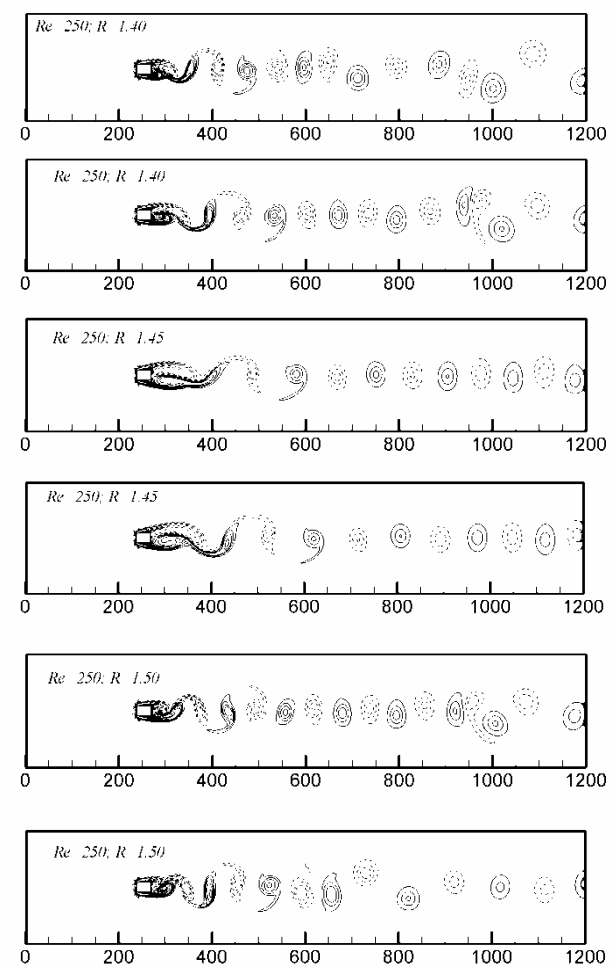

Fig. 19. Vorticity contours around rectangular cylinders with different aspect ratios at $Re = 250$ at two different moments.

$Re = 100$, 150, 200 and 250 are chosen for the study. Special attention is paid to the effects of the aspect ratio on the force coefficients, vortex shedding frequency and the flow structure around the cylinder. The influence of Reynolds number is also discussed. Results are summarized as follows:

There is no local maximum value found at around $R = 0.6$ in the drag coefficient as reported for higher Reynolds numbers in the literature. The drag coefficient generally decreases as the aspect ratio R increases for the aspect ratio range and Reynolds numbers selected. The decreasing rate of the drag coefficient is more distinct in the range of $0.15 \le R \le 2.0$ for all selected Re. However the root-mean-square value of the lift coefficient increases sharply as R increases from 0.15 and reaches a local maximum value at $R \approx 0.5$, and then decreases quickly as R increases.

The Strouhal number St generally decreases with the aspect ratio for $Re = 100$ and 150. For $Re = 200$ and 250, the variation of St with R appears to be more irregular. For $Re = 200$, St reaches a local maximum and minimum at $R = 0.45$ and 1.25 respectively, while for $Re = 250$, St experiences dramatic changes. It decreases sharply first from a higher value near 0.20 at $R = 0.50$ down to a lower value near 0.12 at $R = 1.25$ and then experiences a discontinuity in the range of $1.25 < R < 1.6$ where multiple peaks are found from Fourier spectrum analysis of the lift force and irregular vortex shedding behavior with no fixed shedding frequency is observed from the instantaneous vorticity contours.

The present results using the two-dimensional incompressible lattice Boltzmann method are compared with some existing experimental data and numerical studies. The comparison shows that the LBM can capture the characteristics of the bluff body flow well and is a very useful tool for bluff body flow studies.

Acknowledgment

The work described in this paper was supported by a grant from National Natural Science Foundation of China (Project number No. 90715031). The financial support is gratefully acknowledged.

References

[1] A. Sohankar, C. Norberg and L. Davidson, Simulation of three-dimensional flow around a square cylinder at moderate Reynolds numbers, *Physics of Fluids*, 11 (1999) 288-306.

[2] A. Rokugou, T. Kiwata, A. Okajima, S. Kimura and H. Yamamoto, Numerical analysis of aerodynamic sound radiated from rectangular cylinder, *J. Wind Eng. Ind. Aerodyn.*, 96 (2008) 2203-2216.

[3] A. Sohankar, Large eddy simulation of flow past rectangular-section cylinders: Side ratio effects, *J. Wind Eng. Ind. Aerodyn.*, 96 (2008) 640-655.

[4] Y. Nakamura, Y. Ohya, R. Ozono and R. Nakayama, Experimental and numerical analysis of vortex shedding from elongated rectangular cylinders at low Reynolds numbers $200 - 10^3$, *J. Wind Eng. Ind. Aerodyn.*, 65 (1996) 301-308.

[5] P. W. Bearman and D. M. Trueman, An investigation of the flow around rectangular cylinders, *Aeronaut. Quart.,* 23 (1972) 229-237.

[6] A. Okajima, Strouhal numbers of rectangular cylinders, *J. Fluid Mech.,* 123 (1982) 379-398.

[7] C. Norberg, Flow around rectangular cylinders: Pressure forces and wake frequencies, *J. Wind Eng. Ind. Aerodyn.,* 49 (1993) 187-196.

[8] S. Nakagawa, K. Nitta and M. Senda, An experimental study on unsteady turbulent near wake of a rectangular cylinder in channel flow, *Experiments in Fluids,* 27 (1999) 284-294.

[9] S. Abdollah, A. Mahdi and R. Noorallah, Experimental study of near wake flow behind a rectangular cylinder, *American Journal of Applied Sciences,* 5 (2008) 917-926.

[10] A. Okajima, T. Nagahisa and A. Rokugoh, A numerical analysis of flow around rectangular cylinders, *The Japan Society of Mechanical Engineers, Series II,* 33 (1990) No.4.

[11] N. Kondo and S. Yamada, Third-order upwind finite element computation of the incompressible Navier-Stokes equations Part I. Computation of flow around rectangular

cylinders, *Comput. Methods Appl. Mech. Eng*., 227 (1995) 87-97.

[12] A. Sohankar, C. Norberg and L. Davidson, A numerical study of unsteady two-dimensional flow around rectangular cylinders at incidence, *Internal Report. Chalmers Univeristy of Technology, Depr. Thermo and Fluid Dynamics* (1996) 1-42.

[13] A. Sohankar, C. Norberg and L. Davidson, Numerical simulation of unsteady low-Reynolds number flow around rectangular cylinders at incidence, *J. Wind Eng. Ind. Aerodyn.*, 69-71 (1997) 189-201.

[14] I. Taylor and M. Vezza, Prediction of unsteady flow around square and rectangular section cylinders using a discrete vortex method, *J. Wind Eng. Ind. Aerodyn.*, 82 (1999) 247-269.

[15] K. Shimada and T. Ishihara, Application of a modified model to the prediction of aerodynamic characteristics of rectangular cross-section cylinders, *J. of Fluids and Structures*, 16 (2002) 465-485.

[16] T. Kevin, Lattice Boltzmann simulation of flow around bluff-bodies. *Master Thesis,* Louisiania State University and Agricultural and Mechanical College (2004).

[17] A. Joda, I. Cuesta and A. Vernet, Numerical study of forced convection flow around rectangular cylinders with different side ratios, *Thermal Issues in Emerging Technologies, THETA 1*, Cairo, Egypt (2007) Jan 3-6th.

[18] P. L. Bhatnagar, E. P. Gross and M. Krook, A model for collision processes in gases. 1. small amplitude processes in charged and neutral one-component systems. *Phys. Rev*., 94 (1954) 511-514.

[19] Z. Guo, B. Shi and N. Wang, Lattice BGK model for Incompressible Navier-Stokes equation, *Journal of Computational Physics*, 165 (2000) 288-306.

[20] S. Chapman, T. G. Cowling and D. Burnet, *The mathematical theory of non-uniform gases. an account of the kinetic theory of viscosity, thermal conduction, and diffusion in gases*, Cambridge University Press, 3rd edition (1990).

[21] Y. Dazhi, M. Renwei, L. S. Luo and S. Wei, Viscous flow computations with the method of lattice Boltzmann equation, *Progress in Aerospace Sciences*, 39 (2003) 329-367.

[22] Y. Shimizu and Y. Tanida, Fluid forces acting on cylinders of rectangular cross-section, *Trans. JSME B*, 44 (384) (1978) 2699-2706.

[23] A. Okajima, Numerical analysis of flow around an Oscillating cylinder, *Proc.sixth Int.Conf. On flow induced vibration*, London, U.K (1995)159-166.

[24] R. W. Davis and E. F. Moore, A numerical study of vortex shedding from rectangles, *J. Fluid Mech*., 116 (1982) 475-506.

[25] R. Franke, W. Rodi and B. Schonung, Numerical calculation of laminar vortex shedding flow past cylinders, *J. Wind Eng. Ind. Aerodyn.*, 35 (1990) 237-257.

[26] A. Sohankar, L. Davidson and C. Norberg, Numerical simulation of unsteady flow around a square two-dimensional cylinder, *The Twelfth Australian Fluid Mechanics Conference*, The University of Sydney, Australia (1995) 517-520.

[27] J. Robichuax, S. Balachandar and S. P. Vanka, Three-dimensional floquet instability of the wake of a square cylinder. *Physics of Fluids*, 11 (3) (1999) 560-578.

[28] A. K. Saha, G. Biswas and K. Muralidhar, Three-dimensional study of flow past a square cylinder at low Reynolds numbers, *International Journal of Heat and Fluid Flow*, 24 (2003) 54-66.

Chaoying Zhou is currently a professor in Mechanical Engineering Department, Shenzhen Graduate School, Harbin Institute of Technology. She received her Ph.D. in 1994. Her research interests include flow control of vortex induced vibration, fluid structure interaction, drag reduction of bluff body, application researches including MAV, and wind turbine aerodynamic design.